Biosensors and Bioelectronics 118 (2018) 97–101

Contents lists available at ScienceDirect

Biosensors and Bioelectronics

journal homepage: www.elsevier.com/locate/bios

A solid ionic Lactate biosensor using doped graphene-like membrane of Au-EVIMC-titania nanotubes-polyaniline

Hongying Cheng*, Cuiying Hu, Zhongling Ji, Wangcheng Ma, Hongxia Wang

School of chemical biology and materials engineering, Jiangsu Key Laboratory for Environment Functional Materials, Suzhou University of Science and Technology, Suzhou 215009, Jiangsu, PR China

ARTICLE INFO

Keywords:
Ionic liquid
Titania nanotubes
Lactate dehydrogenase
Enzyme biosensor
Graphene-like

ABSTRACT

Herein, a doped graphene-like membrane was designed, which was copolymerized to be a solid ionic biosensor by using titania nanotubes (TiNTs), polyaniline (PANI), EvimCl (1-ethyl-3-vinylimidazolium chloride, EVIMC) and chloroauric acid ($HAuCl_4$). The structure of graphene-like arrangement and the copolymerization mechanism of the film were discussed in detail. Because of the high catalytic property, Lactate could be determined on the membrane catalyzed by lactate dehydrogenase (LDH) containing isocitrate dehydrogenase (NAD^+), which was immobilized onto the film by electrostatic attraction. The electrochemical response on the LDH/Au-EVIMC-TiNTs-PANI/ITO was increased by twice than the LDH/TiNTs/PANI/ITO, and exhibited two linear responses within the concentration range from 5.5×10^{-7} M to 5.55×10^{-6} M, and 5.55×10^{-6} M to 3.33×10^{-3} M, with a detection limit of 1.65×10^{-7} M ($S / N = 3$). The interference study for other common coexistence such as uric acid and hemoglobin revealed that there was no overlapping signal for the detection of Lactate on the biosensor. The developed method proved the most stability in the determination of real blood samples, and the recoveries ranged from 96.7% to 105.8% with a satisfactory result.

1. Introduction

Recently, the TiNTs with nanoscaled channel have attracted the considerable attraction, because of its high properties, including high surface area, good electronic conductivity, biocompatibility and high chemical stability (Sandoval et al., 2017; Sarswat et al., 2017; Agilan and Rajendran, 2018). Moreover, the TiNTs coupling with PANI has also been chemical oxidized offline, showing the soft skeleton, the crystalline structure (Huang et al., 2015) and the excellent electrocatalytic performance (Zhu et al., 2015). Up to now, the ionic liquids (IL) have the properties such as wide electrochemical window, good biocompatibility and high ionic conductivity. And they have been applied in modified electrodes or biosensors to bind carbon paste or carbon nanotubes (Yang et al., 2015). Apparently, the appropriate selection of IL in polymerization could also improve the rigidity and productivity of the copolymer (Wang et al., 2017) such as PANI.

The measurement of Lactate level was very important, because it could not only benefit for the differential medical diagnosis and therapeutic method, but also assure the quality in dairy products and beverages. Various methods have been reported for the determination of Lactate such as polarimetry (Feng et al., 2010), gas chromatography (GC) (Inoue et al., 2006), capillary electrophoresis (CE) (Alhusban et al., 2014), high performance liquid chromatography (HPLC) (Gómez-Mingot et al., 2012) and nuclear magnetic resonance (NMR) (Seli et al., 2008). While, most were expensive, needed complicated sample pretreatment and trained persons (Pundirn et al., 2016). At this time, biosensing methods attracted the researchers' interests, because they were simple, fast, specific and highly sensitive (Vargas et al., 2016; Naiara et al., 2016). The enzymes utilized to catalyze Lactate included lactate oxidase (LOx) (Hickey et al., 2016) and LDH (Zhang et al., 2016). Because of the diversitied forms, the LDH biosensor coupled with various supports were very widely used.

In this study, the appropriate size of TiNTs was synthesized by the hydrothermal method (Liu et al., 2014). Under the effect of polymerization initiation, the aniline, TiNTs grafted with $-NH_2$ (Wang et al., 2012), EVIMC and $HAuCl_4$ were electro copolymerized on the surface of indium tin oxide (ITO). Several morphology characterizations expressed the copolymerization mechanism, which showing a multi conjugation and a graphene-like arrangement. Under the synergistic and induction effects among the components, the reduced product of $HAuCl_4$ on the graphene-like grids showed the irregular nano scale. And the proposed biosensor presented outstanding electro conductivity, biocompatibility, the stability and the ideal reproducibility in the 400 times determination of Lactate.

* Corresponding author.
E-mail address: chenghy1015@126.com (H. Cheng).

https://doi.org/10.1016/j.bios.2018.07.031
Received 16 June 2018; Received in revised form 8 July 2018; Accepted 16 July 2018
Available online 17 July 2018
0956-5663/

2. Experimental

2.1. Materials and reagents

Nano-TiO_2 powder (P-25) was purchased from Degussa Corporation (USA, 30–50 nm in diameter). EVIMC, $HAuCl_4$ and aniline were obtained from Fluka Chemical Co. (USA). (3-Aminopropyl) triethoxysilane (APTES, 99%) and 2, 2′- Azo - bisisobutyronitrile (AIBN) was obtained from Aladdin Chemical Co. Phosphate buffer solutions (PBS 0.2 mol L^{-1}) were prepared by varying the ratio of NaH_2PO_4 to Na_2HPO_4. ITO glass was purchased from Suzhou Nippon Sheet Glass Electronics Co. Ltd. (Suzhou, China). Ultra-pure water (18.2 MΩ/cm) used throughout the experiments was prepared ourselves.

2.2. Preparation of the Au-EVIMC-TiNTs-PANI/ITO

TiNTs was prepared self-synthesis by a previously reported hydrothermal method (Dai et al., 2010), and the TiNTs-NH_2 was fabricated in mixture solution at room temperature as reported (Cao et al., 2009). The detail information could be seen in the supplemental information.

Before modifying, pieces of ITO glass (1 cm × 5 cm) were cleaned and dried. Then 5uL 0.05 M AIBN was dropped onto the surface and dried in the atmosphere. About 0.0075 g EVIMC (0.01 M) and 10 mg TiNTs-NH_2 were added into 5 mL 0.01 M HCl. After being ultra-sonicated for 30 min, 50uL aniline was added and stirred for 30 min again. Successively, after adding 50uL $HAuCl_4$ in the above mixture in ice bath, the pretreated ITO was subjected to electrochemical polymerization by repeatedly cycling from 0.0 V to + 1.2 V for 15 cycles.

2.3. Fabrication and electrochemical characterization

The enzyme of LDH containing NAD^+ was dropped onto the film of Au-EVIMC-TiNTs-PANI and then was air dried and stored in vacuum at 4 °C designated as LDH/Au-EVIMC-TiNTs-PANI/ITO. For a comparative purpose, other modified electrodes were fabricated as LDH/TiNTs/PANI/ITO, LDH/TiNTs/ITO, and LDH/PANI/ITO.

The Cyclic voltammograms (CVs) and Electrochemical Impedance Spectroscopy (EIS) of the modified electrodes were recorded in 25 mL 0.1 M PBS(pH = 7) containing 5 mM $Fe(CN)_6^{3-/4-}$ and 0.1 M KCl. And the amperometric detection was conducted containing various concentrations of Lactate.

2.4. Pretreatment of blood samples and detection of Lactate

After collection of volunteers', the blood samples were pretreated by heparin to separate the plasma in the cell to avoid the interference from glycolysis. Before detection, 0.5 mL of pretreated plasma was diluted in 5.0 mL of PBS solution. Then the traditional colourimetric method (λ = 550 nm) and this proposed method were used to detect the Lactate to evaluate the practicability of the biosensor.

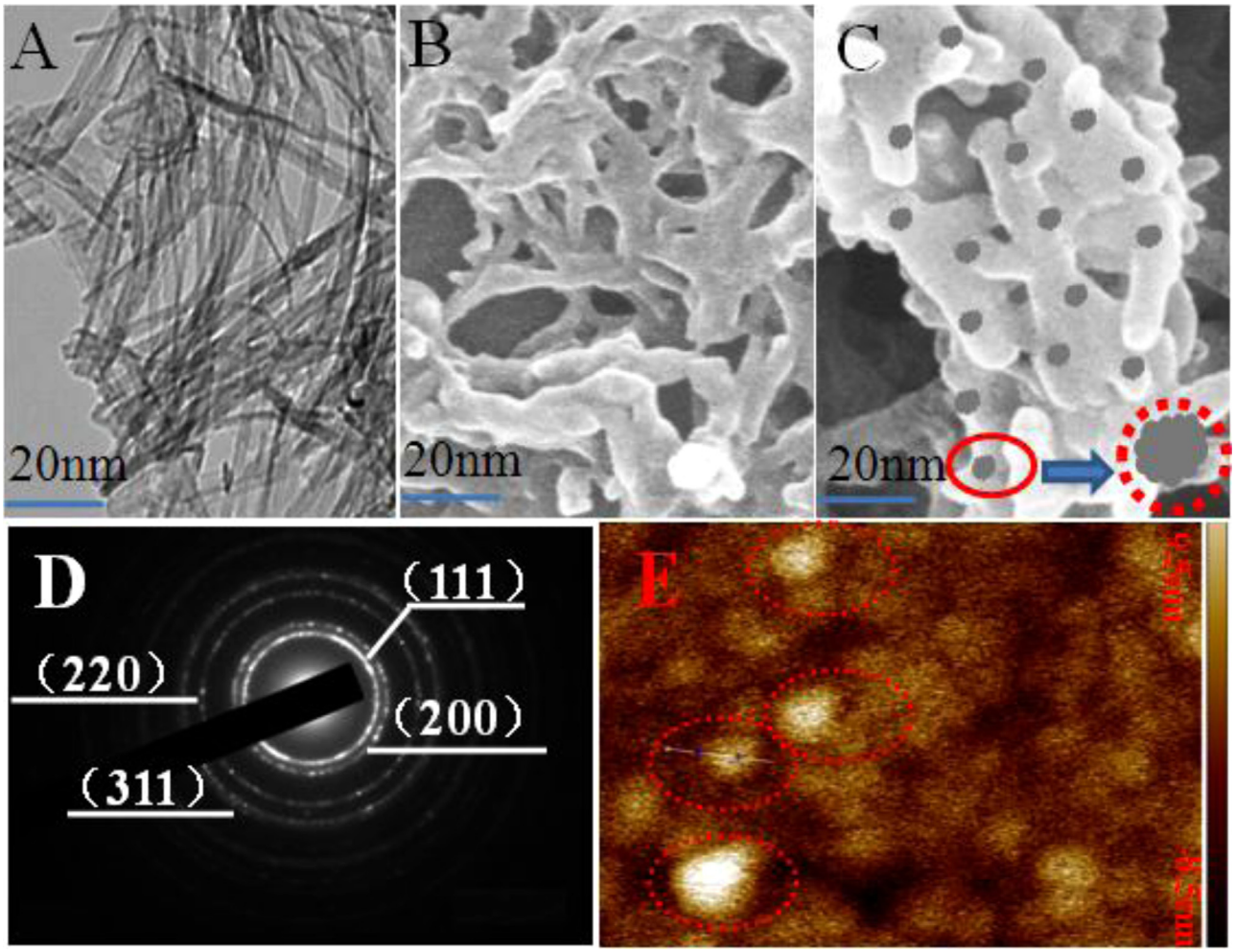

Fig. 1. (A-C) The TEM image of TiNTs, SEM of TiNTS-PANI and Au-EVIMC-TiNTS-PANI, respectively. (D-E) The corresponding SEAD and AFM pattern, respectively. Inset in (C) was the nano-Au SEM shape.

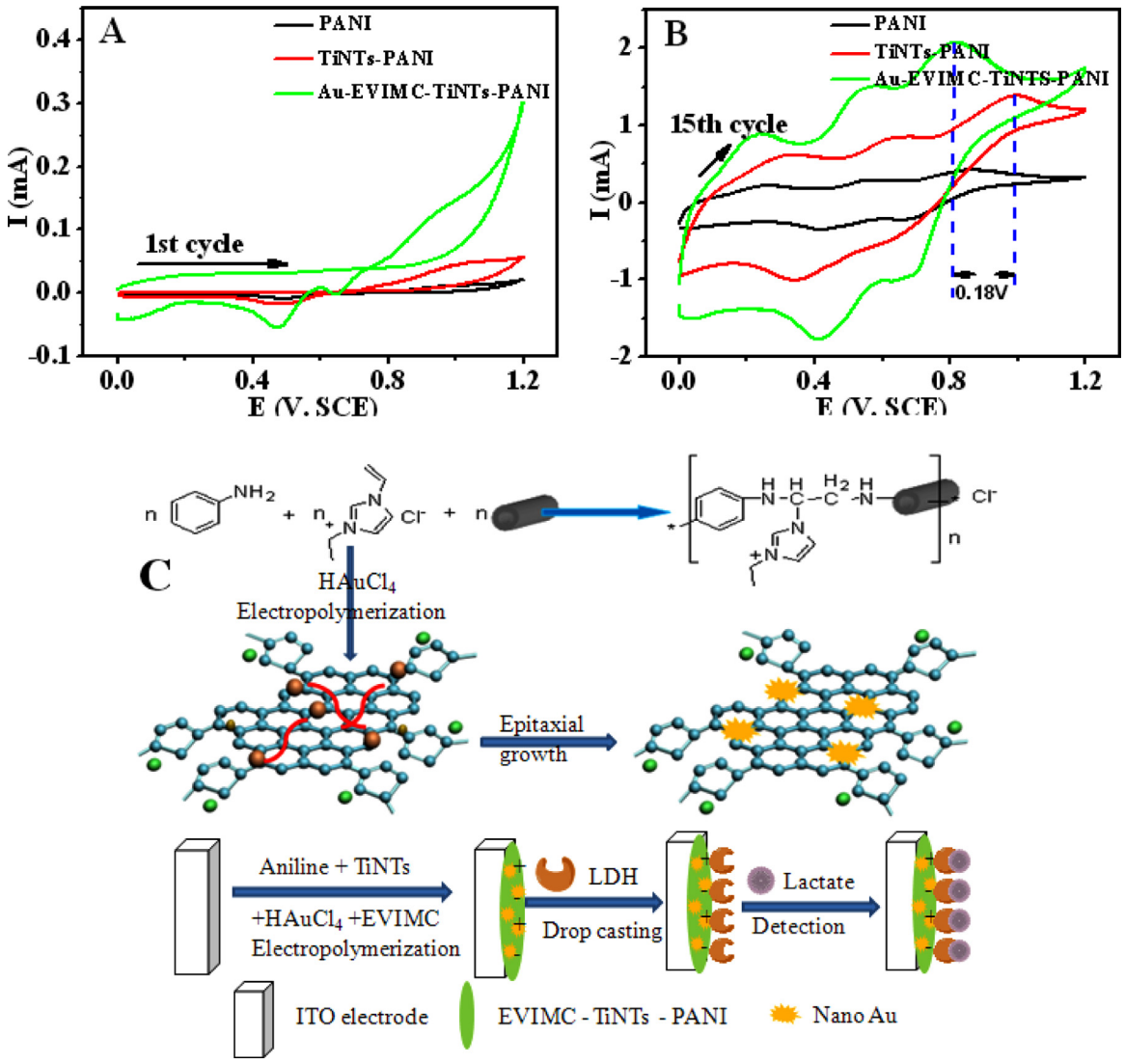

Fig. 2. (A-B) The scanning voltammogram at 1st and 15th cycle, respectively, at a scan rate of 50 mV s^{-1}. (C) Schematic illustration of the copolymerization process of Au-EVIMC-TiNTs-PANI and fabrication of the biosensor.

3. Results and discussion

3.1. Characterization of the biosensor

Fig. 1(A-C) showed the transmission electron microscope (TEM) and scanning electron microscope (SEM) images of the TiNTs, TiNTs-PANI and Au-EVIMA-TINTs-PANI, respectively. As shown, the diameter of bare TiNTs was about 15 ± 2 nm and the edge were smooth and visible clearly. After copolymerization with PANI, the diameter became larger and the shape of TiNTs became vague in Fig. 1B and C. Some nano Au could be seen uniformly attached to the copolymer, which accorded with the clear flare spot of the atomic force microscope (AFM) in Fig. 1E. The inset was the nano Au morphology. Under the synergistic and the induction effect of the components, the nano Au presented irregular shape, implying more active sites available. Fig. 1D showed the selected-area electron diffraction (SEAD) pattern of Au-EVIMC-TiNTs-PANI. The four crystal diffraction planes on (111), (200), (220), and (311) degrees proved the typical polycrystalline nature.

Fig. 2A and B were the CVs recorded during the copolymerization of several components at 1st and 15th cycle scanning, respectively. Obviously, the peak current was found to increase with the number of cycles increasing and the copolymerization of TiNTs-NH_2 and $HAuCl_4$. The three prominent redox couples corresponding to the conversion of leucoemeraldine, emeraldine and pernigraniline form of PANI (Santhosh et al., 2006) became much more obviously. Additionally, the positive and negative shifts of the anodic and cathodic potential resulted from the broadening of electrochemistry window of EVIMC and copolymerization of TiNTs-NH_2. While after $HAuCl_4$ being added, the potential shifted negatively about 0.18 V, which tended to be reversible in Fig. 2B, and the result copolymer was light yellow-green (Pereira et al., 2007).

Then, the surface morphology of LDH/PANI/ITO, LDH/TiNTs/PANI/ITO and LDH/Au-EVIMC-TiNTs-PANI was characterized in Fig. S1(A-C), respectively. Because of the soft skeleton and neat arrangement of PANI, Fig. S1(A) presented smooth. While the irregular arrangement of TiNTs/PANI and the irregular shape of nano Au, Fig. S1(B) and Fig. S1(C) were rough.

3.2. Electrochemical properties of the electrodes

As expected, the peak currents on the modified sensors in Fig. S2(A) were higher than bare ITO. Because of the obstruction of those non-conductive biomacromolecules of enzyme for the electron transference, the peak current lowered and the charge transfer resistances (Rct) showed a largely increased diameter in Fig. S2(B) after LDH modified on the film. Moreover, the peak current ratio of Au-EVIMC-TiNTs-PANI

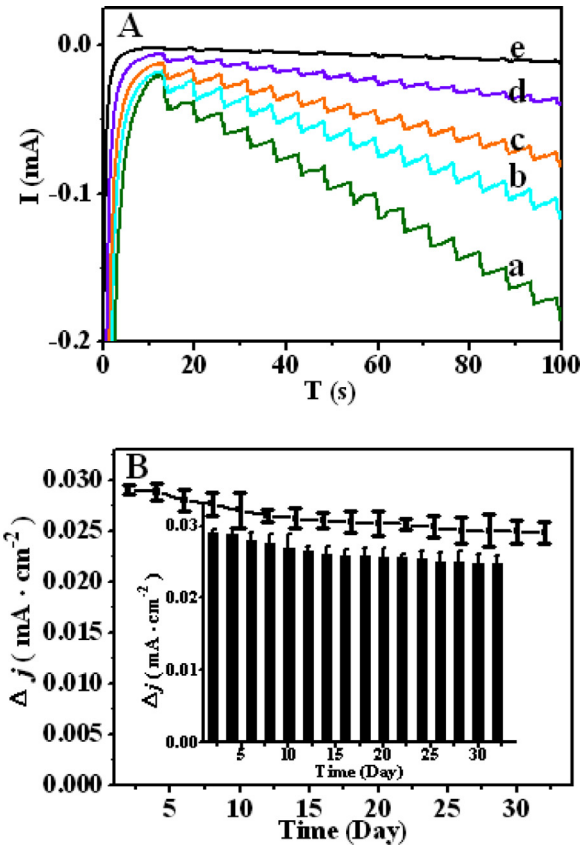

Fig. 3. (A) Amperometric response of the various modified biosensors for the successive addition of Lactate into 0.1 M PBS (pH 7.0) at an applied potential of − 0.05 V; (a) LDH/Au-EVIMC-TiNTs-PANI/ITO; (b) LDH/TiNTs/PANI/ITO; (c) LDH/TiNTs/ITO; (d) LDH/PANI/ITO; (e) bare LDH/ITO. (B) The stability of LDH/Au-EVIMC-TiNTs-PANI/ITO.

to TiNTs/PANI was about 2, resulted from the better catalysis and more pathways for the electron transference on its surface. Comparatively, the Rct of bare ITO showed the least resistance, implying the built of the sensor as expected. All the Rcts had some degree of semicircle domain, implying intrinsic resistance to redox probe.

3.3. Optimization of the component usage

The usage of EVIMC was optimized by monitoring the hardness (Hv) as the formula listed in Scheme S1 and the current density (Δj) shown in Fig. S3(A). When the ratio of IL/aniline was 1.2, the Hv and theΔj presented much better property. In fact, the appropriate charge from EVIMC was benefit to the cross-linking of the LDH and NAD^+ coenzyme because of the electrostatic attraction. But the excessive EVIMC contained more substituents of imidazolium rings in the graphene-like structure, which would loosen the rigidity of polymer.

Of course, the usages of TiNTs-NH_2 and $HAuCl_4$ were also studied. In consideration of homogeneity, stability and rigidity, the ratio of TiNTs-NH_2 to $HAuCl_4$ was controlled as 1.0. In the actual experimental process, the usages of TiNTs-NH_2 and $HAuCl_4$ were chosen as 10 mg and 50 uL, respectively.

Because LDH and NAD^+ coenzyme played important roles in the catalysis to Lactate, the dosages of LDH and NAD^+ were investigated in Fig. S3(B). The excessive dosages of LDH and NAD^+ would result in a thicker membrane impeding the transmission of electrons and the hindrance for the permeation of NADH generated from the reaction of NAD^+. And the sensitivity of the biosensor reached the top at 0.3U of LDH and 0.20% (m/m) of NAD^+.

3.4. Polymerization mechanism of Au-EVIMC-TiNTs-PANI

Some characteristic peaks of EVIMC were found in the fourier transform infrared (FTIR) spectrum of Au-EVIMC-TiNTs-PANI in Fig. S4(A). The 1170 cm^{-1} and 1575 cm^{-1} was the symmetrical telescopic vibration and typical skeleton vibration of imidazole ring, respectively. And the 2950 cm^{-1} was the telescopic vibration of CH_3CH_2- in imidazole ring. Moreover, the weak 3030 cm^{-1} wrapped in the wide peak of hydrogen was the −C−Cl. In addition, the x-ray diffraction (XRD) pattern of the polymer was shown in Fig. S4(B). The results were in good accordance with the SEAD analysis. Furthermore, the peak intensity ratios of (111) and (200) to (220) and (311) were much higher, strongly showing the homogeneous crystal growth along the (111) and (200) directions. These observations confirmed the formation of Au-EVIMC-TiNTs-PANI.

For the lowest energy, the connection between radicals was the copolymerization mechanism as followed in Fig. 2C. On the basis of aromatic ring in PANI, the conjugated six-membered-ring was connected by the some active sites in PANI, −C=C− in the EVIMC and NH_2-grafted on the TiNTs. And the analogue structure of Au-EVIMC-TiNTs-PANI looked like doped graphene. In fact, because of many active sites on the surface of the reduced product, nano Au was probably attached to the ring lattice, retaining the high homogeneity and stability.

3.5. Optimization of determination

According to the reaction of Lactate catalyzed by LDH listed in the formula Scheme S2, the pH had a great degree of influence on the biosensor response for Lactate. So it was investigated in the range of 5.5–8.5 shown in Table S1. The current density reached a maximum value between 7.0 and 8.0. When pH exceeded 8.0, the changing of the mediated electrochemical reactions and the activity of enzyme on the biosensor resulted in the decrease of the sensitivity and the reproducibility on the biosensor. In consideration of the stability of the conjugated ring and the sensitivity of the biosensor, the pH 7.0 was chosen.

The influence of the applied potential on the biosensor was tested in the range of − 300–100 mV. The current increased greatly as the applied potential increasing positively with an excellent signal-to-noise ratio at − 0.05 V. At this potential, some easily oxidizable and reducible species present in real samples became less susceptible, so − 0.05 V versus SCE was chosen as the optimum working potential. The effect of scan rates on the voltammetric behavior was monitored using probe shown in Fig. S5(A-B). As reported (Pereira et al., 2007), the cathodic and anodic peak current were linearly dependent on the logarithm of scan rate (ν) when $\log\nu > 1\ mV\ s^{-1}$, and redox potentials showed dependence on scan rate.

3.6. Amperometric response and application of biosensor for the analysis of Lactate

Fig. 3A displayed the amperometric response of the various modified electrodes for the successive addition of 0.5 mM Lactate into 5 mL 0.1 M PBS (pH 7.0). As expected, the different response represented the different catalytic property of the film. Because of the high catalytic property of Au-EVIMC-TiNTs-PANI, the increase of the current at the proposed biosensor was significantly higher than at other electrodes. The current density presented two good linearities: Δj ($mA\ cm^{-2}$) = 0.0074 + 1.424 C (mM) (R = 0.9897), Δj ($mA\ cm^{-2}$) = 0.01531 + 0.09535 C (mM) (R = 0.998) in the concentration range of 5.5×10^{-7} M to 5.55×10^{-6} M, and 5.55×10^{-6} M to 3.33×10^{-3} M, respectively, with a detection limit of 1.65×10^{-7} M (S/N = 3) shown in Fig. S6(A). At the biosensor, the steady current could reach within 8 s because of the stable doped graphene-like structure with high sensitivity and catalytic activity.

Even more, the stability of the developed biosensor was examined through 12 successive measurements every three days by using single

biosensor (immersed in buffer at ambient temperature in intervals) and the parallel biosensors reserved in 4 °C for different time displayed in Fig. 3B, showing a relative standard deviation (RSD) of 1.8% (n = 12). The total ideal number of determination nearly reached 400 times, and then attenuated gradually along with the use.

The biosensor's practicability was tested by direct detecting Lactate in real plasma samples, and compared with the reference method listed in Table S2. Just as expected, the data had preferable correlation from the two methods. Then the recoveries were tested (n = 4) by adding a series of standard solutions of Lactate in above serum sample, which ranged in 96.7–105.8% with RSD less than 3.16%. These results validated reliable analytical performance of our biosensor.

To evaluate the selectivity of this biosensor, different potential interferents present in real plasma sample such as glucose, uric acid and hemoglobin were added successively and tested as shown in Fig. S6B. The results showed that this biosensor had a greater tolerance from those interferents, and could be used for the determination of the Lactate in real samples.

4. Conclusions

An intensified, solid and ionic biosensor has been successfully designed for determination of Lactate. The doped graphene-like structure of Au-EVIMC-TiNTs-PANI strengthened the rigidity, improved the stability and enhanced the electrocatalytic property of the film. And this proposed biosensor exhibited good reproducibility, rapid response time, wide linear range and ultralow detection limit, which was used for the real serum detection with satisfactory results. Although the activity of the enzyme immobilized on the proposed biosensor will be influenced greatly on the effects of temperature and acidity. The doped graphene-like film with superior catalytic activity, sensitivity and stability could be extended for the detection of other biomolecules in the early diagnosis of diseases.

Acknowledgements

This work was financially supported by the Jiangsu Natural Science Foundation of China (13KJB150035) and Agricultural Infrastructure Project of Suzhou Science and Technology Development Plan (Grant no. SYN201507).

Appendix A. Supporting information

Supplementary data associated with this article can be found in the online version at doi:10.1016/j.bios.2018.07.031.

References

Sandoval, A., Zanella, R., Klimova, T.E., 2017. Catal. Today 282, 140–150.
Sarswat, P.K., Mishra, Y.K., Free, M.L., 2017. Biosens. Bioelectron. 89, 334–342.
Agilan, P., Rajendran, N., 2018. Appl. Surf. Sci. 439, 66–74.
Huang, H., Gan, M.Y., Ma, L., Yu, L., Hu, H.F., Yang, F.F., Li, Y.J., Ge, C.Q., 2015. J. Alloy. Compd. 630, 214–221.
Zhu, J., Liu, X.Q., Wang, X.H., Huo, X.H., Yan, R., 2015. Sens. Actuators B Chem. 221, 450–457.
Yang, J., Wang, Q., Zhang, M., Zhang, S., Zhang, L., 2015. Food Chem. 187, 1–6.
Wang, S., Shi, Q.X., Ye, Y.S., Wang, Y., Peng, H.Y., Xue, Z.G., Xie, X.L., Mai, Y.W., 2017. Electrochim. Acta 245, 1010–1022.
Feng, L.D., Sun, B., Bian, X.C., Chen, Z.M., Chen, X.S., 2010. Polym. Test. 29, 771–776.
Inoue, Y., Shinka, T., Ohse, M., Ikawa, H., Kuhara, T., 2006. J. Chromatogr. B 838, 37–42.
Alhusban, A.A., Gaudry, A.J., Breadmore, M.C., Gueven, N., Guijt, R.M., 2014. J. Chromatogr. A 1323, 157–162.
Gómez-Mingot, M., Alcaraz, L.A., MacIntyre, D.A., Jiménez, B., Pineda-Lucena, A., Montiel, V., Banks, C.E., Iniesta, J., 2012. Anal. Methods 4, 284–290.
Seli, E., Botros, L., Sakkas, D., Burns, D.H., 2008. Fertil. Steril. 90, 2183–2189.
Pundirn, C.S., Narwal, V., Batra, B., 2016. Biosens. Bioelectron. 86, 777–790.
Vargas, E., Ruiz, M.A., Campuzano, S., GonzálezdeRivera, G., López-Colino, F., Reviejo, A.J., Pingarrón, J.M., 2016. Talanta 152, 147–154.
Naiara, H.I., Leticia, G.C., Vicente, M., Christopher, W.F., Craig, E.B., Jesús, I., 2016. Biosens. Bioelectron. 77, 1168–1174.
Hickey, D.P., Reid, C.R., Milton, R.D., Minteer, S.D., 2016. Biosens. Bioelectron. 77, 26–31.
Zhang, X.M., Ding, S.S., Cao, S.M., Zhu, A.W., Shi, G.Y., 2016. Biosens. Bioelectron. 80, 315–322.
Liu, N., Chen, X.Y., Zhang, J.L., Schwank, J.W., 2014. Catal. Today 225, 34–51.
Wang, H.X., Zhou, Y.H., Guo, Y.J., Liu, W.J., Dong, C., Wu, Y.H., Li, S.D., Shuang, S.M., 2012. Sens. Actuators B Chem. 163, 171–178.
Dai, H., Chi, Y.W., Wu, X.P., Wang, Y.M., Wei, M.D., Chen, G.N., 2010. Biosens. Bioelectron. 25, 1414–1419.
Cao, H.N., He, J., Deng, L., Gao, X.Q., 2009. Appl. Surf. Sci. 255, 7974–7980.
Santhosh, P., Manesh, K.M., Gopalan, A., Lee, K.P., 2006. Anal. Chim. Acta 575, 32–38.
Pereira, A.C., Aguiar, M.R., Kisner, A., Macedo, D.V., Kubot, L.T., 2007. Sens. Actuators B Chem. 124, 269–276.